

Persistent Paramagnons Deep in the Metallic Phase of $\text{Sr}_{2-x}\text{La}_x\text{IrO}_4$

H. Gretarsson,¹ N. H. Sung,¹ J. Porras,¹ J. Bertinshaw,¹ C. Dietl,¹ Jan A. N. Bruin,¹ A. F. Bangura,¹ Y. K. Kim,^{2,3,4} R. Dinnebier,¹ Jungho Kim,⁵ A. Al-Zein,⁶ M. Moretti Sala,⁶ M. Krisch,⁶ M. Le Tacon,^{1,7} B. Keimer,¹ and B. J. Kim¹

¹Max-Planck-Institut für Festkörperforschung, Heisenbergstr. 1, D-70569 Stuttgart, Germany
²Advanced Light Source, Lawrence Berkeley National Laboratory, Berkeley, California 94720, USA
³Center for Correlated Electron Systems, Institute for Basic Science, Seoul 151-742, South Korea
⁴Department of Physics and Astronomy, Seoul National University, Seoul 151-747, South Korea
⁵Advanced Photon Source, Argonne National Laboratory, Argonne, Illinois 60439, USA
⁶European Synchrotron Radiation Facility, BP 220, F-38043 Grenoble Cedex, France
⁷Karlsruher Institut für Technologie, Institut für Festkörperphysik, Hermann-v.-Helmholtz-Platz 1, D-76344 Eggenstein-Leopoldshafen, Germany

(Received 24 March 2016; revised manuscript received 7 June 2016; published 1 September 2016)

We have studied the magnetic excitations of electron-doped $\text{Sr}_{2-x}\text{La}_x\text{IrO}_4$ ($0 \leq x \leq 0.10$) using resonant inelastic x-ray scattering at the Ir L_3 edge. The long-range magnetic order is rapidly lost with increasing x , but two-dimensional short-range order (SRO) and dispersive magnon excitations with nearly undiminished spectral weight persist well into the metallic part of the phase diagram. The magnons in the SRO phase are heavily damped and exhibit anisotropic softening. Their dispersions are well described by a pseudospin-1/2 Heisenberg model with exchange interactions whose spatial range increases with doping. We also find a doping-independent high-energy magnetic continuum, which is not described by this model. The spin-orbit excitons arising from the pseudospin-3/2 manifold of the Ir ions broaden substantially in the SRO phase, but remain largely separated from the low-energy magnons. Pseudospin-1/2 models are therefore a good starting point for the theoretical description of the low-energy magnetic dynamics of doped iridates.

DOI: 10.1103/PhysRevLett.117.107001

The proximity of two-dimensional antiferromagnetism and high-temperature superconductivity in copper oxides [1] and iron pnictides [2] suggest that both phases are intimately related. Neutron scattering [3,4] and resonant inelastic x-ray scattering (RIXS) [5] experiments on both sets of materials [6–11] have indeed revealed damped spin excitations in the superconducting regimes of the phase diagrams. In RIXS experiments, their dispersions and spectral weights are closely similar to those of magnons in the magnetically ordered parent compounds.

The notion of magnetically mediated high-temperature superconductivity has motivated an extensive search for new materials that realize two-dimensional quantum antiferromagnets akin to those in the undoped cuprates and iron pnictides. The antiferromagnetic Mott insulator Sr_2IrO_4 has emerged as a particularly promising candidate, because it is isostructural to La_2CuO_4 , the progenitor of one of the most prominent families of superconducting cuprates, and it exhibits a closely analogous electronic structure. The Mott-insulating state in Sr_2IrO_4 is driven by the combination of intra-atomic spin-orbit coupling and electronic correlations (“spin-orbit Mott insulator”). Its magnetic ground state and low-energy magnetic excitations are well described by the pseudospin $j_{\text{eff}} = 1/2$ states arising from the spin-orbit coupled spin and orbital angular momenta of the iridium ions [12,13]. The pseudospins decorate a square lattice, and their interactions are well described by a Heisenberg model

[14] akin to the spin-1/2 Hamiltonian describing the magnetic dynamics of La_2CuO_4 [15].

These similarities are driving theoretical work predicting d -wave superconductivity in electron-doped Sr_2IrO_4 [16–19]. Evidence supporting this prediction has emerged from angle-resolved photoemission spectroscopy (ARPES) measurements on electron-doped Sr_2IrO_4 surfaces, doped by charge transfer from a monolayer of adatoms. The Fermi surface of the surface electron system is split up into disjointed segments (“Fermi arcs”) [20] and exhibits a gap with d -wave symmetry at low temperature [21,22]—features that are hallmarks of d -wave superconductivity in the hole-doped cuprates [1]. These results have also been partially reproduced in $\text{Sr}_{2-x}\text{La}_x\text{IrO}_4$ [23], although impurity-driven disorder [24] and oxygen vacancies [25] have been an impediment to the progress in bulk, chemically doped counterparts.

Despite these encouraging results, it is still unclear whether the magnetic correlations are as robust against carrier doping in Sr_2IrO_4 as they are in the cuprates. In particular, the on-site Coulomb repulsion is relatively weak in Sr_2IrO_4 , resulting in a small charge gap (~ 0.4 eV [26]), which is comparable to the magnon bandwidth [14]. Recent Raman experiments have also revealed a strong pseudo-spin-lattice coupling in Sr_2IrO_4 , indicating unquenched orbital dynamics that is quite unusual for a Mott insulator [27]. These observations indicate a complex interplay

between pseudospin, charge, and lattice degrees of freedom. All of these variables are expected to be sensitive to chemical doping, highlighting the need for a systematic study on how the magnetic correlations evolve in electron-doped Sr_2IrO_4 .

Here we report a systematic investigation of the doping evolution of the magnetic structure and magnetic excitations in $\text{Sr}_{2-x}\text{La}_x\text{IrO}_4$ ($x = 0, 0.015, 0.04, \text{ and } 0.10$) by Ir L_3 edge RIXS. Our results show that antiferromagnetic long-range order (LRO) is rapidly lost upon electron doping ($0.015 < x_c \leq 0.04$), followed by persistent two-dimensional short-range order (SRO) deep in the metallic phase of $\text{Sr}_{2-x}\text{La}_x\text{IrO}_4$. We report a detailed description of the low-energy magnon and high-energy spin-orbit exciton in the SRO phase, which provides an excellent basis for the theoretical description of the electronic properties of the doped iridates.

The RIXS experiments were carried out at the European Synchrotron Radiation Facility using the ID20 beam line. A spherical (2 m radius) diced Si(844) analyzer with a 60 mm mask and a Si(844) secondary monochromator were used to obtain an overall energy resolution of ~ 25 meV (full width at half maximum) and an in-plane momentum resolution of ~ 0.035 reciprocal lattice units. [The momentum transfer $Q = (H, K, L)$ is quoted in terms of reciprocal vector $\pi/(a, b, c)$ where $a \approx b \approx 3.88$ Å (undistorted unit cell) and $c \approx 25.8$ Å are the lattice parameters. In-plane crystal momenta q are quoted in square-lattice notation with unit lattice constant.] ARPES measurements were performed at beam line 4.0.3 at the Advanced Light Source. The energy of the incident light was $h\nu = 90$ eV and overall energy resolution of ~ 25 meV was achieved. Single crystals of La-doped Sr_2IrO_4 were grown by the flux method, previously described in detail [25]. The La concentrations were checked via electron probe microanalysis.

The physical properties of Sr_2IrO_4 are very sensitive to the doping level and to the crystal growth conditions [24,25,28]. We have therefore carefully characterized all samples using susceptibility and resonant x-ray diffraction measurements. Figure 1(a) shows the phase diagram derived from our magnetization measurements (see Supplemental Material [29]). In crystals with $x = 0$ and 0.015, the long-range magnetic order [13] sets in around $T_N = 240$ and 230 K, respectively, while no signature of such order is found in both $x = 0.04$ and 0.10, indicating a doping-induced transition into a paramagnetic state. This observation is confirmed by monitoring the antiferromagnetic Bragg peaks, which are visible in the elastic scattering channel of the RIXS spectra for $Q_M = (0.5, 0.5, L_{\text{even}})$ [Fig. 1(b)]. Whereas in the $x = 0$ and 0.015 crystals the magnetic Bragg peaks are sharp and narrow along the HH directions, the elastic magnetic response of the $x = 0.04$ and $x = 0.10$ samples becomes extremely broad along the HH direction and no correlations are observed along the L direction (see Supplemental Material [29]), implying two-dimensional

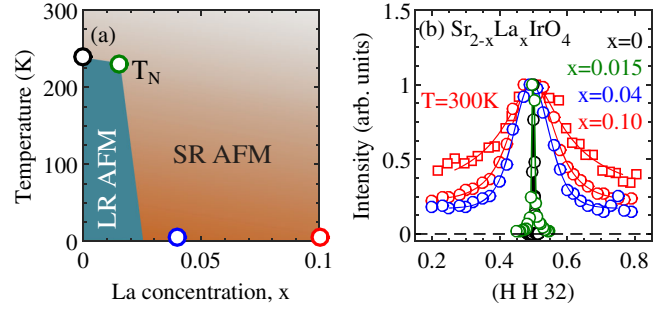


FIG. 1. (a) Schematic phase diagram of $\text{Sr}_{2-x}\text{La}_x\text{IrO}_4$. Data points for the Néel temperature are taken from the magnetization measurements in Ref. [29]. (b) HH scans through the magnetic Bragg peak $Q_M = (0.5, 0.5, L_{\text{even}})$ at $T = 20$ K (includes $x = 0.10$ at $T = 300$ K). The maximum intensity of each scan was normalized to unity.

(2D) magnetic short-range order. By fitting the profiles to 2D Lorentzians, we determined the in-plane correlation lengths $\xi = 10$ and 8 Å for $x = 0.04$ and $x = 0.10$, respectively [30]. We also note that the 2D magnetic correlations persist to high temperature ($\xi \sim 5$ Å for $x = 0.10$ at $T = 300$ K), consistent with the large in-plane exchange coupling determined by RIXS and Raman scattering [14,27].

The rapid suppression of magnetic LRO in electron-doped $\text{Sr}_{2-x}\text{La}_x\text{IrO}_4$ [see Fig. 1(a)] agrees with neutron diffraction results from Ref. [[24]] and parallels the behavior in hole-doped cuprates (such as $\text{La}_{2-x}\text{Sr}_x\text{CuO}_4$), where the LRO is quenched for $x \sim 0.02$ [31]. In the electron-doped cuprates, on the other hand, LRO survives well above 0.1 electrons per Cu [32]. This supports the analogy between electron doping in the iridates and hole doping in the cuprates proposed on the basis of the opposite signs of the next-nearest-neighbor hopping amplitudes in the two sets of materials [16].

Having studied the static magnetic properties, we now turn to the evolution of the magnetic excitations in $\text{Sr}_{2-x}\text{La}_x\text{IrO}_4$ across the transition between the LRO and SRO phases. Figures 2(a) and 2(b) display color maps of RIXS spectra ($x = 0$ and $x = 0.10$) taken at $T = 20$ K along high-symmetry directions of reciprocal space. In agreement with prior work on the undoped compound [14], the data show a highly dispersive magnon excitation emanating from the antiferromagnetic ordering vector and extending up to about 0.2 eV. Our new data on the highest doped compound show that magnon excitations (paramagnons) with closely similar dispersion and nearly undiminished spectral weight persist deep into the phase diagram of $\text{Sr}_{2-x}\text{La}_x\text{IrO}_4$. The magnetic dynamics in the doped iridates are thus strongly reminiscent of those in the hole-doped layered cuprates, where paramagnon excitations akin to the spin waves of antiferromagnetic La_2CuO_4 were found deeply in the metallic and superconducting regimes of the phase diagram [6,7].

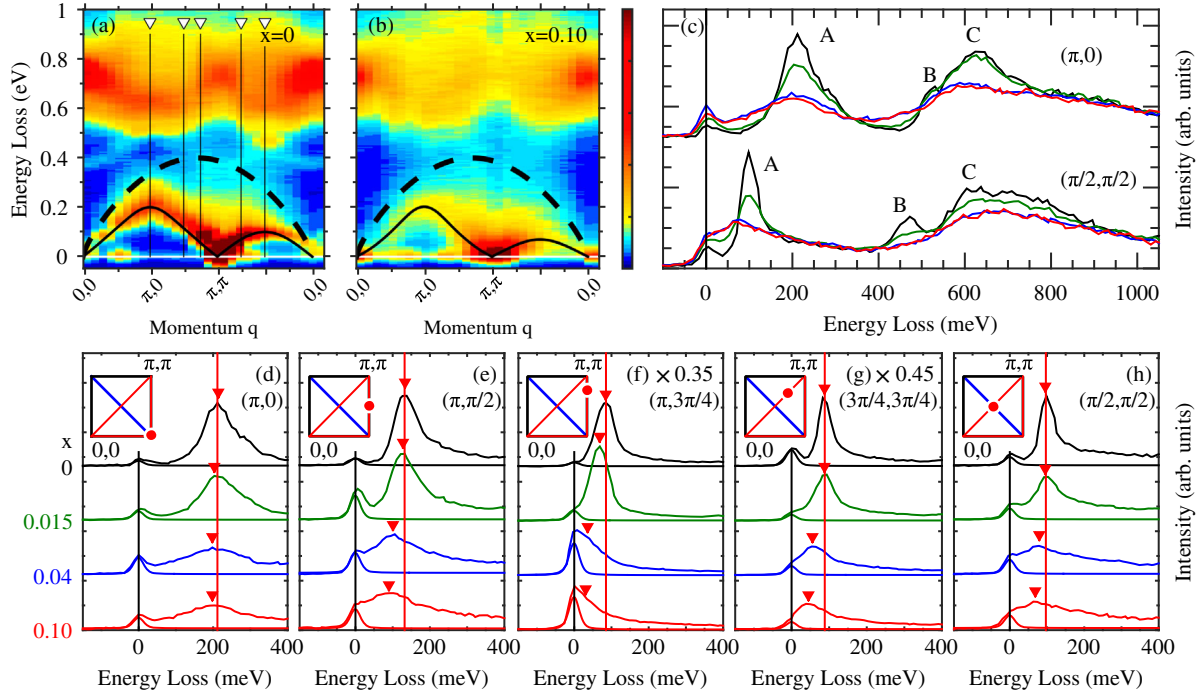


FIG. 2. RIXS intensity maps of $\text{Sr}_{2-x}\text{La}_x\text{IrO}_4$ taken along high symmetry directions for (a) $x = 0$ and (b) $x = 0.10$. The intensity is in arbitrary units and starts from zero. Data were collected at $T = 20$ K. The spectral weight around 1 eV was used to normalize the RIXS spectra of different samples. The solid black lines are taken from the fit in Fig. 3 and the dashed black line is a guide to the eye, representing the upper boundary of the doping-independent continuum. Constant-momentum cuts for all samples are displayed in (c) for $q = (\pi, 0)$ and $q = (\pi/2, \pi/2)$. Letters refer to the excitations discussed in text. (d)–(h) Comparison of individual low-energy RIXS spectra for different doping levels and crystal momenta [see black vertical lines in (a)]. Red circles in insets show the q in the Brillouin zone of the undistorted tetragonal unit cell (black square), the magnetic cell (blue line) is also shown. The contribution from elastic scattering has been superimposed on each spectrum. The red triangles represent the maximum intensity of the magnon modes (see text for details), and the vertical red line the magnon energy for the parent compound.

To emphasize the importance of our findings, we show in Fig. 3(a) an ARPES intensity map in the $x = 0.10$ sample, taken at $T = 10$ K and at the Fermi level energy (E_F). Despite the detection of well-defined paramagnons in the $x = 0.10$ sample a clear Fermi surface (FS) is apparent, indicating that the sample is deep in the metallic phase [33]. The dispersive charge excitation, crossing E_F , can be seen in more detail in Fig. 3(b), where we plot the binding energy as a function of momentum [taken along the dashed

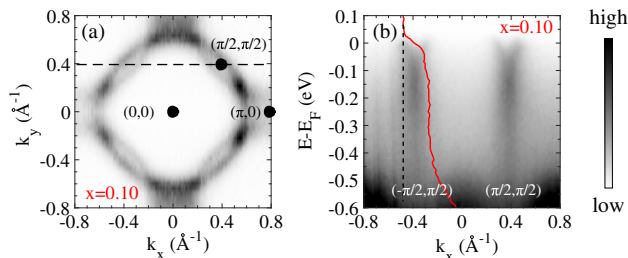


FIG. 3. (a) ARPES intensity map showing the Fermi surface of the $x = 0.10$ sample. (b) Cut along the dashed horizontal line in (a). The red solid line shows the energy distribution curve at the momentum (vertical dashed line) where the dispersive charge excitations reach the Fermi level (E_F).

horizontal line in (a)]. In a previous report [23], it has been shown that this band is gapped near $(\pi, 0)$, making it a Fermi arc instead of a usual FS. Investigating how the magnetic correlations can coexist with a FS (i.e., system with Fermi-Dirac statistics), similar to the case in optimally hole-doped cuprates, is a question that should be addressed. One possible explanation for this discrepancy could be electronic phase separation on a macroscopic scale. This would give rise to a RIXS spectrum that looks like a superposition of metallic and insulating parts which is not supported by our data [e.g., Fig. 2(f) shows no hint of a parent phase in the $x = 0.10$ sample]. Microscopic phase separation, as seen in STM measurements on metallic $\text{Sr}_{2-x}\text{La}_x\text{IrO}_4$ [24], can, however, not be excluded.

To gain more insight into magnetic excitations it is important to look systematically at how the RIXS spectra evolve with increasing doping. Figure 2(c) presents two salient features of the magnon (A) in the constant-momentum cuts plots ($x = 0, 0.015, 0.04$, and $x = 0.10$). First, the magnon energy at $q = (\pi, 0)$ remains unchanged, although the magnon becomes severely damped. Second, at $q = (\pi/2, \pi/2)$, the magnon shows clear softening in addition to becoming broader. The observed anisotropic magnetic softening along the $(0, 0) \rightarrow (\pi, \pi)$ direction is in

stark contrast to the hardening of the magnon in electron-doped cuprates, but resembles results seen in the metallic Bi-based cuprates [34,35]. This strengthens the analogy between electron-doped iridates and hole-doped cuprates already pointed out above.

To quantify the doping dependence of the magnon (or paramagnon) dispersion relations, we have tracked the peak positions in the RIXS spectra as a function of momentum [e.g., red triangles in Figs. 2(d)–2(h)]. The resulting dispersions are plotted in Fig. 4. The error bars were determined by selecting the energy interval in which the measured intensity is within 95% of the maximum intensity, following a recent RIXS study of a doped cuprate [36]. Whereas elastic and inelastic contributions could be reliably separated in most of the spectra, the magnon peak positions for $q = (0, 0)$ and $q = (\pi, \pi)$ could not be accurately determined due to the low intensity of the magnetic signal and the strong elastic line, respectively. These q points were therefore not included in the dispersions in Fig. 4.

To obtain the doping dependent magnetic interactions, we have fitted the magnon dispersions obtained in this way by a Heisenberg model with exchange interactions between first, second, and third nearest neighbors in the IrO_2 planes, termed J , J' , J'' . For the $x = 0$ and $x = 0.015$ samples, we obtain $J = 60$, $J' = -20$, and $J'' = 15$ meV, in excellent agreement with prior work on undoped Sr_2IrO_4 (solid lines in Fig. 4) [14]. To describe the anisotropic softening of the magnon dispersion in the $x = 0.04$ and 0.10 samples noted above, the fit parameters were altered to $J = 48$, $J' = -27$, and $J'' = 20$ meV (dashed lines in Fig. 4); here, the ratio between J' and J'' was fixed in order to reduce the free parameters. Doping Sr_2IrO_4 with electrons thus reduces the nearest-neighbor exchange interaction by $\sim 20\%$, while enhancing the longer-range interactions by $\sim 30\%$. This finding is in general accord with expectations for magnetic interactions in itinerant-electron systems, and it will guide future theoretical work on electronic correlations in doped iridates.

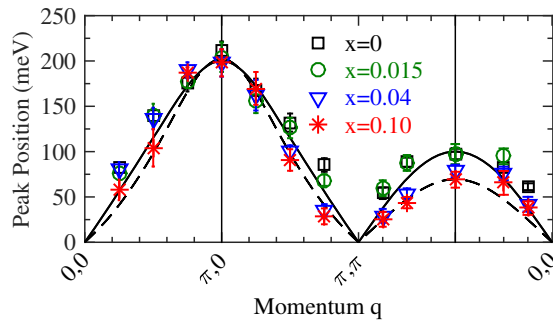


FIG. 4. Experimental magnon dispersion at $T = 20$ K for different doping levels. The solid (dashed) line represents the result of the best fit for $x = 0$ and 0.015 ($x = 0.04$ and 0.10), with parameters stated in the text.

The intensity maps in Figs. 2(a) and 2(b) and constant-momentum cuts in Figs. 2(d)–2(h) highlight yet another intriguing feature of this 2D quantum magnet. By looking at the doping dependence at $(\pi/2, \pi/2)$, it becomes clear that the magnetic excitation has two components: the sharp mode discussed above which reacts strongly to electron-doping, and a high-energy tail which retains its intensity upon doping [e.g., Fig. 2(c)]. This momentum dependent high-energy tail is bounded at low energies by the magnon dispersion, and at high energies by the dashed black line in Figs. 2(a) and 2(b). The same behavior is also evident along the Brillouin zone border [e.g., Fig. 2(e)]. One explanation for this marked departure in doping behavior between the single magnon and the high-energy tail is that the latter arises from spinonlike excitations not directly associated with the Néel-ordered state. Indeed, in the cuprates, the spinon-picture [37] has been evoked to explain the strong damping of the magnon at $(\pi, 0)$ [38] and the pronounced asymmetrical line shape of the two-magnon Raman scattering [39,40]. The latter was recently also observed in Sr_2IrO_4 [27]. Although this analogy and explanation are intriguing, further measurements, targeting the polarization dependence of the signal [41] are required to determine the origin of the high-energy magnetic tail in Sr_2IrO_4 .

For excitation energies above the optical gap (> 0.4 eV), we find a dispersive spin-orbit exciton mode arising from the $j_{\text{eff}} = 3/2$ pseudospin manifold [14,26]. In the parent compound, this feature comprises a sharp excitation near the optical gap [marked B in Fig. 2(c)] followed by incoherent higher-energy excitations (marked C). As pointed out in Ref. [42], the broadening of feature C may be due to overlap with the particle-hole continuum. Upon La doping, the dispersion of the spin-orbit excitons ($B + C$) becomes less pronounced, and the sharp feature B disappears. At $(\pi/2, \pi/2)$, in particular, feature B is drastically suppressed upon doping, while C loses intensity. The strong damping of the spin-orbit exciton can be attributed to a lowering of the particle-hole continuum threshold as the system becomes metallic.

In summary, our systematic RIXS measurements of electron-doped $\text{Sr}_{2-x}\text{La}_x\text{IrO}_4$ have uncovered persistent short-range magnetic order deep in the metallic phase of $\text{Sr}_{2-x}\text{La}_x\text{IrO}_4$ accompanied by dispersive magnetic excitations (paramagnons) of nearly undiminished spectral weight. Both the persistence of magnonlike excitations upon doping and their anisotropic softening indicate an intriguing analogy between electron-doped iridates and hole-doped cuprates. The low-energy magnon dispersions are well described by a $j_{\text{eff}} = 1/2$ Heisenberg model with exchange interactions whose spatial range increases with increasing doping. A doping independent high-energy magnetic continuum has also been found, suggesting that the ground state of Sr_2IrO_4 contains additional short-range correlations not captured by the Heisenberg model. Finally, the $j_{\text{eff}} = 3/2$ spin-orbit exciton broadens and becomes

less dispersive with increasing doping, but the overlap with the low-energy paramagnon branch remains small. Models based on $j_{\text{eff}} = 1/2$ pseudospins therefore appear to be a good starting point for the theoretical description of the electronic structure and for a realistic assessment of the prospects for unconventional superconductivity in doped iridates.

We would like to thank G. Jackeli, G. Khaliullin, and R. Coldea for fruitful discussions. N. H. Sung was supported by the Alexander von Humboldt Foundation. We acknowledge financial support by the DFG under Grant No. TRR80.

Note added.—Damped magnon and anisotropic softening have recently also been observed by Liu and collaborators in La-doped Sr_2IrO_4 [43].

-
- [1] B. Keimer, S. A. Kivelson, M. R. Norman, S. Uchida, and J. Zaanen, *Nature (London)* **518**, 179 (2015).
- [2] J. Paglione and R. L. Greene, *Nat. Phys.* **6**, 645 (2010).
- [3] M. Fujita, H. Hiraka, M. Matsuda, M. Matsuura, J. M. Tranquada, S. Wakimoto, G. Xu, and K. Yamada, *J. Phys. Soc. Jpn.* **81**, 011007 (2012).
- [4] J. M. Tranquada, G. Xu, and I. A. Zaliznyak, *J. Magn. Magn. Mater.* **350**, 148 (2014).
- [5] L. J. P. Ament, M. van Veenendaal, T. P. Devereaux, J. P. Hill, and J. van den Brink, *Rev. Mod. Phys.* **83**, 705 (2011).
- [6] M. Le Tacon *et al.*, *Nat. Phys.* **7**, 725 (2011).
- [7] M. P. M. Dean, G. Dellea, R. S. Springell, F. Yakhou-Harris, K. Kummer, N. B. Brookes, X. Liu, Y.-J. Sun, J. Strle, T. Schmitt, L. Braicovich, G. Ghiringhelli, I. Božović, and J. P. Hill, *Nat. Mater.* **12**, 1019 (2013).
- [8] M. Minola, G. Dellea, H. Gretarsson, Y. Y. Peng, Y. Lu, J. Porras, T. Loew, F. Yakhou, N. B. Brookes, Y. B. Huang, J. Pellicciari, T. Schmitt, G. Ghiringhelli, B. Keimer, L. Braicovich, and M. Le Tacon, *Phys. Rev. Lett.* **114**, 217003 (2015).
- [9] K. Ishii, M. Fujita, T. Sasaki, M. Minola, G. Dellea, C. Mazzoli, K. Kummer, G. Ghiringhelli, L. Braicovich, T. Tohyama, K. Tsutsumi, K. Sato, R. Kajimoto, K. Ikeuchi, K. Yamada, M. Yoshida, M. Kurooka, and J. Mizuki, *Nat. Commun.* **5**, 3714 (2014).
- [10] W. S. Lee, J. J. Lee, E. A. Nowadnick, S. Gerber, W. Tabis, S. W. Huang, V. N. Strocov, E. M. Motoyama, G. Yu, B. Moritz, H. Y. Huang, R. P. Wang, Y. B. Huang, W. B. Wu, C. T. Chen, D. J. Huang, M. Greven, T. Schmitt, Z. X. Shen, and T. P. Devereaux, *Nat. Phys.* **10**, 883 (2014).
- [11] K.-J. Zhou, Y.-B. Huang, C. Monney, X. Dai, V. N. Strocov, N.-L. Wang, Z.-G. Chen, C. Zhang, P. Dai, L. Patthey, J. van den Brink, H. Ding, and T. Schmitt, *Nat. Commun.* **4**, 1470 (2013).
- [12] B. J. Kim, H. Jin, S. J. Moon, J.-Y. Kim, B.-G. Park, C. S. Leem, Jaejun Yu, T. W. Noh, C. Kim, S.-J. Oh, J.-H. Park, V. Durairaj, G. Cao, and E. Rotenberg, *Phys. Rev. Lett.* **101**, 076402 (2008).
- [13] B. J. Kim, H. Ohsumi, T. Komesu, S. Sakai, T. Morita, H. Takagi, and T. Arima, *Science* **323**, 1329 (2009).
- [14] J. Kim, D. Casa, M. H. Upton, T. Gog, Y.-J. Kim, J. F. Mitchell, M. van Veenendaal, M. Daghofer, J. van den Brink, G. Khaliullin, and B. J. Kim, *Phys. Rev. Lett.* **108**, 177003 (2012).
- [15] R. Coldea, S. M. Hayden, G. Aeppli, T. G. Perring, C. D. Frost, T. E. Mason, S.-W. Cheong, and Z. Fisk, *Phys. Rev. Lett.* **86**, 5377 (2001).
- [16] F. Wang and T. Senthil, *Phys. Rev. Lett.* **106**, 136402 (2011).
- [17] Y. Yang, W.-S. Wang, J.-G. Liu, H. Chen, J.-H. Dai, and Q.-H. Wang, *Phys. Rev. B* **89**, 094518 (2014).
- [18] H. Watanabe, T. Shirakawa, and S. Yunoki, *Phys. Rev. Lett.* **110**, 027002 (2013).
- [19] Z. Y. Meng, Y. B. Kim, and H.-Y. Kee, *Phys. Rev. Lett.* **113**, 177003 (2014).
- [20] Y. K. Kim, O. Krupin, J. D. Denlinger, A. Bostwick, E. Rotenberg, Q. Zhao, J. F. Mitchell, J. W. Allen, and B. J. Kim, *Science* **345**, 187 (2014).
- [21] Y. K. Kim, N. H. Sung, J. D. Denlinger, and B. J. Kim, *Nat. Phys.* **12**, 37 (2016).
- [22] Y. J. Yan, M. Q. Ren, H. C. Xu, B. P. Xie, R. Tao, H. Y. Choi, N. Lee, Y. J. Choi, T. Zhang, and D. L. Feng, *Phys. Rev. X* **5**, 041018 (2015).
- [23] A. de la Torre, S. McKeown Walker, F. Y. Bruno, S. Ricco, Z. Wang, I. Gutierrez Lezama, G. Scheerer, G. Giriat, D. Jaccard, C. Berthod, T. K. Kim, M. Hoesch, E. C. Hunter, R. S. Perry, A. Tamai, and F. Baumberger, *Phys. Rev. Lett.* **115**, 176402 (2015).
- [24] X. Chen, T. Hogan, D. Walkup, W. Zhou, M. Pokharel, M. Yao, W. Tian, T. Z. Ward, Y. Zhao, D. Parshall, C. Opeil, J. W. Lynn, V. Madhavan, and S. D. Wilson, *Phys. Rev. B* **92**, 075125 (2015).
- [25] N. H. Sung, H. Gretarsson, D. Pröpper, J. Porras, M. Le Tacon, A. V. Boris, B. Keimer, and B. J. Kim, *Philos. Mag.* **96**, 413 (2016).
- [26] S. J. Moon, H. Jin, W. S. Choi, J. S. Lee, S. S. A. Seo, J. Yu, G. Cao, T. W. Noh, and Y. S. Lee, *Phys. Rev. B* **80**, 195110 (2009).
- [27] H. Gretarsson, N. H. Sung, M. Höppner, B. J. Kim, B. Keimer, and M. Le Tacon, *Phys. Rev. Lett.* **116**, 136401 (2016).
- [28] M. Ge, T. F. Qi, O. B. Korneta, D. E. De Long, P. Schlottmann, W. P. Crummett, and G. Cao, *Phys. Rev. B* **84**, 100402(R) (2011).
- [29] See Supplemental Material at <http://link.aps.org/supplemental/10.1103/PhysRevLett.117.107001> for magnetization measurements, L-dependence of the magnetic peak, and resistivity measurements.
- [30] We cannot rule out that the broadening of the Bragg reflections is partially due to unresolved incommensurability of the magnetic correlations, in analogy to the hole-doped cuprates. The values of the correlation length we quote should therefore be regarded as lower bounds.
- [31] B. Keimer, N. Belk, R. J. Birgeneau, A. Cassanho, C. Y. Chen, M. Greven, M. A. Kastner, A. Aharony, Y. Endoh, R. W. Erwin, and G. Shirane, *Phys. Rev. B* **46**, 14034 (1992).
- [32] N. P. Armitage, P. Fournier, and R. L. Greene, *Rev. Mod. Phys.* **82**, 2421 (2010).

- [33] A weakly metallic behavior is seen in transport measurement on the $x = 0.04$ sample [29], indicating that the insulator to metal phase boundary occurs close to that doping level.
- [34] M. Guarise, B. Dalla Piazza, H. Berger, E. Giannini, T. Schmitt, H. M. Rønnow, G. A. Sawatzky, J. van den Brink, D. Altenfeld, I. Eremin, and M. Gioni, *Nat. Commun.* **5**, 5760 (2014).
- [35] M. P. M. Dean, A. J. A. James, A. C. Walters, V. Bisogni, I. Jarrige, M. Hücker, E. Giannini, M. Fujita, J. Pellicciari, Y. B. Huang, R. M. Konik, T. Schmitt, and J. P. Hill, *Phys. Rev. B* **90**, 220506 (2014).
- [36] H. Y. Huang, C. J. Jia, Z. Y. Chen, K. Wohlfeld, B. Moritz, T. P. Devereaux, W. B. Wu, J. Okamoto, W. S. Lee, M. Hashimoto, Y. He, Z. X. Shen, Y. Yoshida, H. Eisaki, C. Y. Mou, C. T. Chen, and D. J. Huang, *Sci. Rep.* **6**, 19657 (2016).
- [37] C.-M. Ho, V. N. Muthukumar, M. Ogata, and P. W. Anderson, *Phys. Rev. Lett.* **86**, 1626 (2001).
- [38] N. S. Headings, S. M. Hayden, R. Coldea, and T. G. Perring, *Phys. Rev. Lett.* **105**, 247001 (2010).
- [39] S. Sugai, M. Sato, T. Kobayashi, J. Akimitsu, T. Ito, H. Takagi, S. Uchida, S. Hosoya, T. Kajitani, and T. Fukuda, *Phys. Rev. B* **42**, 1045 (1990).
- [40] A. A. Katanin and A. P. Kampf, *Phys. Rev. B* **67**, 100404 (2003).
- [41] B. Dalla Piazza, M. Mourigal, N. B. Christensen, G. J. Nilsen, P. Tregenna-Piggott, T. G. Perring, M. Enderle, D. F. McMorrow, D. A. Ivanov, and H. M. Rønnow, *Nat. Phys.* **11**, 62 (2015).
- [42] Jungho Kim, M. Daghofer, A. H. Said, T. Gog, J. van den Brink, G. Khaliullin, and B. J. Kim, *Nat. Commun.* **5**, 4453 (2014).
- [43] X. Liu, M. P. M. Dean, Z. Y. Meng, M. H. Upton, T. Qi, T. Gog, Y. Cao, J. Q. Lin, D. Meyers, H. Ding, G. Cao, and J. P. Hill, *Phys. Rev. B* **93**, 241102(R) (2016).